Dynamics of the magnetic flux trapped in fractal clusters of normal phase in a superconductor

Yu. I. Kuzmin*
Ioffe Physical Technical Institute of the Russian Academy of Sciences, 26 Polytechnicheskaya Street, Saint Petersburg 194021, Russia
(Received 7 February 2001; revised manuscript received 16 March 2001; published 14 August 2001)

The influence of geometry and morphology of superconducting structure on critical currents and magnetic flux trapping in percolative type-II superconductors is considered. The superconductor contains clusters of normal phase, which act as pinning centers. It is found that such clusters have significant fractal properties. The main features of these clusters are studied in detail: the cluster statistics is analyzed, the fractal dimension of their boundary is estimated, the distribution of critical currents is obtained, and its peculiarities are explored. It is examined thoroughly how the finite-resolution capacity of the cluster geometrical size measurement affects the estimated value of the fractal dimension. The effect of fractal properties of the normal phase clusters on the electric field arising from magnetic flux motion is investigated in the case of an exponential distribution of cluster areas. The voltage-current characteristics of superconductors in the resistive state for an arbitrary fractal dimension are obtained. It is revealed that the fractality of the boundaries of the normal phase clusters intensifies the magnetic flux trapping and thereby raises the critical current of a superconductor.

DOI: 10.1103/PhysRevB.64.094519 PACS number(s): 74.60.Ge, 74.60.Jg, 05.45.Df, 61.43.Hv

I. INTRODUCTION

An important property of clusters of normal phase in a superconductor consists in their capability to trap a magnetic flux. By virtue of their capacity to hold the vortices from moving under the action of the Lorentz force, such clusters can act as effective pinning centers.[1–4] This feature is used widely in the making new composite superconducting materials of high-current-carrying capability.[5,6] The morphological characteristics of clusters of normal phase exert an appreciable effect on the magnetic flux dynamics in superconductors, especially when the clusters have fractal boundaries.[7–9] In the present work the geometric probability properties of such fractal clusters are considered in detail, and their influence on the dynamics of trapped magnetic flux and critical currents is analyzed.

The notion of a fractal as an object of fractional dimension was first introduced by Mandelbrot[10] and has received a lot of applications in various domains of science.[11–14] The fractal approach has been found to be most useful in an investigation of inhomogeneous materials. There are many possibilities, both the determinate fractals and the stochastic ones to be formed in composite superconductors. As an example of the first kind the multilayered structures prepared by electron-beam deposition of superconductor (Nb) and normal metal (Cu) layers with a fractal stacking sequence on sapphire substrates can be mentioned.[15] In order to obtain stochastic fractal clusters, it is essential that a process like diffusion-limited aggregation would take place in the course of the synthesis of materials.[14] A similar process can be realized, for instance, when thin films are evaporated. So in Ref. 16 films of fractal structure have been grown by vapor deposition of Au on silicon substrates with a silicon nitride buffer sublayer. It is worthy of note that porous, random, or highly ramified clusters are not necessarily all fractals. A fractal cluster has such a property that its characteristic measures (in what follows, the perimeter and the enclosed area) have to obey a certain scaling law that includes an exponent named the fractal dimension.[11,14]

Fractal clusters can be also formed in such highly inhomogeneous materials as high-temperature superconductors (HTS's). So the fractal dissipative regime has been observed in high-resolution measurements of the dynamical resistance of $(BiPb)_2Sr_2Ca_2Cu_3O_{10+y}$ (BPSCCO) composites containing normal phase inclusions of Ag.[8,17] The fractal properties of the normal phase clusters contained in $YBa_2Cu_3O_{7-x}$ (YBCO) films, which were prepared by magnetron sputtering on sapphire substrates with a cerium oxide buffer sublayer, have been found in Ref. 9. Percolation clusters provide another example of fractals in superconductors.[18] Although, mathematically, the percolation cluster is a fractal at the threshold point only, the fractal approach works well for any clusters which have a scaling feature.[19] In that case normal phase clusters may be formed by the inclusion of different chemical compositions, as well as domains of the reduced superconducting order parameter can act as such clusters.[8,20] The existence of fractal inclusions of this kind can be demonstrated by fractal dissipation, which has been observed in nontextured polycrystalline YBCO and GdBCO bulk samples.[8] The fractal structure of clusters near the percolation threshold in epitaxial YBCO films has been fully considered in Ref. 21. Of special interest are the works of Surdeanu *et al.*[3,4] where the fractal penetration of magnetic flux in thin HTS films has been investigated by the use of magneto-optics. Epitaxial $Tl_2Ba_2CuO_{6+x}$ films were grown by magnetron sputtering on $SrTiO_3$ substrates, and YBCO films were prepared by pulsed laser deposition on $NdGaO_3$ substrates. The cluster structure of such films is clearly visible in the atomic force microscopy picture published in Ref. 4, whereas the magnetic flux penetrating into the sample from the outside has a well-definite fractal front.

A further consideration will be concerned with the superconductor containing fractal inclusions of a normal phase, which are out of contact with one another. Let us assume that these inclusions are oriented in such a way that their extent along one of the directions far exceeds other linear sizes. Similar columnar defects are of most interest for creating artificial pinning centers.[6,9,22–24] When such a superconduct-

ing structure is cooled below the critical temperature in the magnetic field along the direction of the longest size of these inclusions, the magnetic flux will be frozen in the normal phase clusters. Even after the external field has been turned off, the flux trapped in these clusters is kept unchanged due to the currents that are steadily circulating around them through the superconducting loops. The distribution of the trapped magnetic flux resulting from such a magnetization in the field-cooling regime will be two dimensional. A similar distribution can easily be realized in superconducting films where normal phase inclusions are created during the growth process at the sites of defects on the boundary with the substrate in such a way that their orientation is normal to the surface of the film.[6,23,24] Let us suppose that the film surface fraction covered by the normal phase is below the percolation threshold for the transfer of magnetic flux [50% for two-dimensional (2D) percolation[25]]. In this case the relative portion of the superconducting phase exceeds the percolation threshold, so there is a superconducting percolation cluster in the plane of the film where a transport current can flow. Such a structure provides for effective pinning and thereby raises the critical current, because the magnetic flux is locked in finite clusters of a normal phase, and so the vortices cannot leave them without crossing the surrounding superconducting space. If the transport current is passed through the sample, the trapped magnetic flux remains unchanged as long as the vortices are still held in the normal phase clusters. When the current is increased, the magnetic flux starts to break away from the clusters of pinning force weaker than the Lorentz force created by the transport current. As this takes place, the vortices will first pass through the weak link, which connect the normal phase clusters between themselves.

Such weak links form readily in HTS characterized by an extremely short coherence length. Various structural defects, which would simply cause some additional scattering at long coherence length, give rise to the weak links in HTS. There is a hierarchy of weak links over a wide range of scales in HTS.[6,26–29] At an atomic level the weak links are formed by the structural atomic defects, primarily, by oxygen vacancies.[27,30] It is significant that just these vacancies arisen from the oxygen atom deficit underlie the origin of HTS phenomenon by itself. On a mesoscopic scale twin boundaries are mainly responsible for weak link existence.[28,31–35] Twins form especially readily in YBCO superconductors inasmuch as their unit cell is only close to the orthorhombic one. The twins can be spaced up to several nanometers apart, so even single crystals may have the fine substructure caused by twins. The effect of twins on the magnetic flux motion in HTS has been studied by many authors.[32–40] It is known that the HTS magnetization depends strongly on the orientation of twin plans with respect to the applied magnetic field.[37] It has been found that the flux can easily move along twin plans but not crosswise.[33,34,38] A strong anisotropy of magnetic flux motion along and across twins has been also observed in thin HTS films.[39] At the present time, it is well established that magnetic flux can penetrate easily along the weak links formed by twins.[34,35,40] At last, on a macroscopic scale there are manifold structural defects which can form

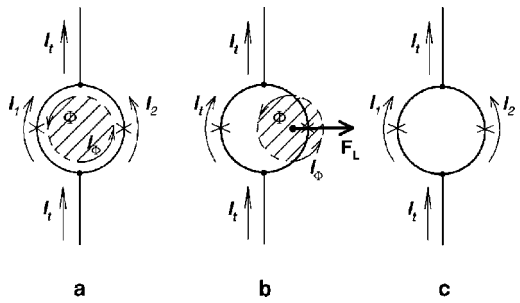

FIG. 1. Schematic representation for the magnetic flux exit from a normal phase cluster through the weak link. For simplicity a single weak link is shown in each branch of the superconducting loop around the normal phase inclusion. Here $I_t=I_1+I_2$ is the transport current, I_Φ is the current related to the trapped magnetic flux Φ, and $\mathbf{F}_L$ is the Lorentz force. (a) The magnetic flux remains trapped in the cluster as long as $I_2+I_\Phi<I_c$, where I_c is the critical current of the weak link. (b) As soon as $I_2+I_\Phi \geqslant I_c$ the Lorentz force expels the flux through the right weak link which has become resistive. (c) As a result the cluster does not contain the magnetic flux anymore, whereas the weak link in the right branch is superconducting anew (provided that $I_2<I_c$).

weak links, which may be grain or crystallite boundaries as well as barriers arising from the secondary degrading the nonstoichiometric crystal into the domains with a high and low content of oxygen.[29,30,41] Moreover, a magnetic field further reduces the coherence length,[42] thus resulting in more easy weak link formation. In conventional low-temperature superconductors, which are characterized by a large coherence length, weak links can be formed due to the proximity effect in sites of minimum distance between the next normal phase clusters.

As soon as the transport current is turned on, this one is added to all the persistent currents, which maintain the magnetic flux to be trapped [Fig. 1(a)]. Each of these currents, such as I_Φ in Fig. 1, is circulating through the superconducting loop around the normal phase cluster wherein the corresponding portion of the magnetic flux is trapped. The loop contains weak links that join the adjacent normal phase clusters transversely to the path of the current. As the transport current is increased, there will come a point when the overall current flowing through the weak link will exceed the critical value, so this link will turn into a resistive state. As this takes place, the space distribution of the currents throughout the superconducting cluster is changed in such a way that the resistive subcircuit will be shunted by the superconducting paths where weak links are not damaged yet [Fig. 1(b)]. The magnetic field created by this redistributed transport current acts via the Lorentz force on the current circulating around the normal phase cluster. As a consequence, the magnetic flux trapped therein will be forced out through the resistive weak link, which has become permeable to the vortices [Figs. 1(b) and 1(c)].

This paper is organized as follows: The geometric statistical properties of the normal phase clusters in YBCO superconducting films are studied, and the fractal dimension of their boundaries is estimated in Sec. II. The dependence of the trapped magnetic flux on the transport current as well as

the pinning gain caused by the cluster fractality are analyzed in Sec. III. The voltage-current (V-I) characteristics of superconductors containing fractal clusters of a normal phase are obtained in Sec. IV. A geometric probability analysis of the weak link distribution over the cluster perimeter is made in Appendix A. Some mathematical details concerning the V-I characteristics are presented in Appendix B.

II. FRACTAL GEOMETRY OF NORMAL PHASE CLUSTERS

Thus, whatever the microscopic nature of weak links may be, they form the channels for vortex transport. It appears that according to their configuration each normal phase cluster has its own value of the critical current of depinning, which contributes to the overall statistical distribution. When a transport current is gradually increased, the vortices will break away first from clusters of small pinning force and, therefore, of small critical current. Thus the decrease in the trapped magnetic flux $\Delta\Phi$ is proportional to the number of all normal phase clusters of critical currents less than a preset value I. Therefore, the relative decrease in the trapped flux can be expressed with the cumulative probability function $F=F(I)$ for the distribution of the critical currents of clusters:

$$\frac{\Delta\Phi}{\Phi}=F(I), \quad \text{where} \quad F(I)=\Pr\{\forall I_j<I\}. \tag{1}$$

The right-hand side of Eq. (1) is the probability that any jth cluster has a critical current I_j less than a given upper bound I.

On the other hand, the magnetic flux trapped in a single cluster is proportional to its area A, so the decrease in the total trapped flux can be represented by the cumulative probability function $W=W(A)$ for the distribution of the areas of the normal phase clusters, which is a measure of the number of clusters of area smaller than a given value of A:

$$\frac{\Delta\Phi}{\Phi}=1-W(A), \quad \text{where} \quad W(A)=\Pr\{\forall A_j<A\}. \tag{2}$$

The distribution function $W=W(A)$ of the cluster areas can be found by a geometric probability analysis of electron photomicrographs of superconducting films.[23] In the most general way the cluster area distribution can be described by a gamma distribution.[43] In the practically important case of YBCO films containing columnar defects[23,24,44] the exponential distribution is realized:

$$W(A)=1-\exp\left(-\frac{A}{\overline{A}}\right), \tag{3}$$

where $\overline{A}$ is the mean area of the cluster.

Thus, in order to clear up how the transport current acts on the trapped magnetic flux, it is necessary to find out the relationship between the distribution of the critical currents of the clusters [Eq. (1)] and the distribution of their areas [Eq. (2)]. To do this, the geometric size of the normal-phase cluster has to be related to its critical current. It seems natural that the pinning force is weaker for larger clusters. Hence, the current is smaller at which the magnetic flux ceases to be trapped inside the cluster and leaves it through the weak links in the form of vortices driven by the Lorentz force. The exit of a vortex from a normal phase cluster can be treated as a problem of a random walk particle reaching an absorbing border.[45] However, unlike the classical problem of the distribution of the exit points (see, e.g., Ref. 46), here the boundary of the area is not absorbing all over, but there are only discrete absorption points, which are randomly arranged along the cluster perimeter. These points of absorption are located just at the sites where weak links are going out on the boundary of the cluster. Hereafter we shall call them the points of entry of vortices into weak links or, simply, entry points. In addition to that, the situation is complicated by the fractality of the cluster boundary as well as by the fact that a random walker is permanently subjected to the Lorentz force.

For simplicity suppose that after the vortex reaches the entry point it passes all the way between two adjacent normal phase clusters without being trapped inside the weak link itself. Here the magnetic flux is transferred by Josephson vortices. The Josephson penetration depth is large enough in the considered materials so that the size of the region, where the vortex is localized, greatly exceeds the characteristic length of all possible structural defects that can occur along the transport channel. Thus the probability that such a vortex will be trapped in passing through a weak link under the action of the Lorentz force is very small. This assumption agrees well with the results of research on magnetic flux motion along weak links,[2,35,47,48] including twins.[33,34,38,40] At the same time, it allows us to highlight the role played by the cluster boundary in the magnetic flux trapping.

Next, we shall consider the simplest case of a uniform distribution of entry points over the cluster perimeter with the distribution function

$$\Psi(l)=\frac{1}{P}, \tag{4}$$

which gives the density of probability to find a weak link at the point l on the perimeter of the complete length P (see Appendix A). Also suppose that the concentration of entry points into weak links per unit perimeter length is constant for all clusters regardless of their size. For the uniform distribution of Eq. (4) this concentration n is independent of the point position, so the mean number of entry points, $\overline{N}$, along the cluster perimeter is proportional to its length:

$$\overline{N}=\oint n(l)\,dl=nP. \tag{5}$$

Finally, let us assume that all clusters are statistically self-similar and that all clusters of equal perimeter have the same pinning force and, therefore, equal critical current.

In order to find the relationship between the size of a cluster and its critical current, we have to solve such a question: what quantity should be used as a measure of the cluster size? Obviously, both the area and the perimeter length

(along with any increasing functions of these values) provide such a measure. At the same time, the cluster area is a measure of the magnetic flux trapped inside. Eventually, to clear up how the transport current affects the trapped flux, the critical current must be related to the area of the cluster.

On the other hand, the pinning force corresponds to such a current at which the vortices break away from the cluster. As the transport current is increasing, the Lorentz force, which expels the magnetic flux, increases as well. The vortex leaves the normal phase cluster when the Lorentz force becomes greater than the pinning force. At the same time, growing in current will result in a redistribution of the magnetic flux, which will penetrate deeper and deeper into a transition layer on that side of the surrounding superconducting space where the Lorentz force is directed [see Fig. 1(b)]. The flux penetration into this transition layer has a fractal behavior, but unlike the case considered in Refs. 3 and 4, the flux front is built up on the fractal phase boundary. In order to leave the normal phase cluster, vortices have to reach the entry points. The exit of the magnetic flux can be considered as the result of random walks of vortices driven by the Lorentz force, which is pushing them into weak links. A similar approach has been successfully used in Ref. 2, where the extreme fronts of the magnetic flux penetrating in a 1D superconducting quantum interference device (SQUID) array were found.

Undoubtedly, it is necessary to keep in mind that real Josephson vortices arise only when magnetic flux enters into weak links, which causes the supercurrents in the transition layer to redistribute.[49] When the random walk vortex, which has not reached the entry point yet, is mentioned, it is primarily meant that the equivalent space distribution of supercurrents creates the same magnetic field. This fact—that the fractal cluster coastline is highly ''indented''—causes the entry points to differ in accessibility for vortices depending on their position on the boundary—they are located in ''skerries'' or on ''protuberances.''[50] It may occur that a vortex will not enter the weak link at all, but to the contrary will stick in some ''dead end.'' In the most simple approach the following outcomes of the random walks may happen: (a) the vortex enters the weak link and leaves the normal phase cluster, (b) the vortex does not enter the weak link and continues its random walks, and (c) the vortex does not enter the weak link and remains to be locked in the ''dead end.'' The wider the transition layer, where the magnetic flux penetrates as the current increases, the more entry points become accessible for vortices. The mean number of entry points, $\overline{N}$, available on the cluster perimeter provides the probability measure of the number of the random walk outcomes, which are favorable for the vortex to go out. In the case of the uniform entry point distribution of Eq. (4) and at a constant concentration of weak links for all clusters, from Eq. (5) it follows that $\overline{N} \propto P$; thus the perimeter length also represents the probability measure of the amount of favorable outcomes for the vortex to leave the cluster. The more entry points into weak links are accessible for random walk vortices, the smaller is the Lorentz force required to expel the flux from a cluster. Hence, we may write the following relationship between the critical current of the cluster and its geometric size:

$$I \propto \frac{1}{\overline{N}} \propto \frac{1}{P}. \tag{6}$$

Thus this expression is true for the simplest case of a uniform distribution of entry points, which is assumed to be the same for all clusters (see Appendix A). Such a simplification allows us to emphasize that in the case being considered the magnetic flux is held in the normal phase cluster by its boundary.

Thus, to deal with the distribution function of Eq. (1), the relation between the perimeter and area of clusters should be studied. It might be natural to suppose that the perimeter-area relation obeys the well-known geometric formula $P \propto \sqrt{A}$. However, it would be a very rough approximation only,[23,24] because this relationship holds for Euclidean geometric objects but on no account for the fractals. As was first found in Ref. 9, the fractal nature of the normal phase clusters exerts an appreciable effect on the dynamics of a magnetic flux in superconductors. For fractal clusters a relation between the perimeter and area has the form

$$P \propto A^{D/2}, \tag{7}$$

where D is the fractal dimension of the cluster perimeter (so-called coastline dimension).[11]

The relation of Eq. (7) is consistent with the generalized Euclid theorem,[11,12] which states that the ratios of the corresponding measures are equal when reduced to the same dimension. Hence it follows that $P^{1/D} \propto A^{1/2}$, which is valid both for Euclidean clusters (the Hausdorff-Besicovitch dimension of their perimeter coincides with the topological one: $D=1$) and for fractal clusters (the Hausdorff-Besicovitch dimension of their boundary strictly exceeds the topological dimension of a line: $D>1$).

The fractal dimension value can be estimated by means of a regression analysis of the sampling of the areas and perimeters of the normal phase clusters. Such a geometric probability analysis was carried out by the procedure described in Ref. 9. For this purpose an electron photomicrograph of YBCO film prepared by magnetron sputtering, which was similar to that published earlier in Ref. 24, has been scanned. The perimeters and areas of clusters have been measured by covering their digitized pictures with a square grid of spacing 60×60 nm^2. The results of the statistical treatment of these data are presented in Table I. The normal phase has occupied 20% of the total surface only, so the transport current can flow through the sufficiently dense percolation superconducting cluster. The primary sampling contains 528 normal phase clusters located on the scanned region of a total area of 200 μm^2. The distribution of the cluster areas is fitted well to the exponential cumulative probability function of Eq. (3) with a mean cluster area $\overline{A}=0.0765$ μm^2. All points of the primary sampling are marked by crosses in plot 1 of Fig. 2, which shows the perimeter-area relation for the normal phase clusters. Figure 2 also demonstrates such an important peculiarity of this relation: the scaling law of Eq. (7) is valid in the

TABLE I. Statistics of normal phase clusters and estimation of the fractal dimension.

Sampling size	Primary sampling 528	Truncated sampling 380
Mean A (μm^2)	0.0765	0.1002
Sample standard deviation of A (μm^2)	0.0726	0.0729
Standard error of estimate for A (μm^2)	3.16×10^{-3}	3.74×10^{-3}
Total scanned A (μm^2)	40.415	38.093
Min value of A (μm^2)	2.07×10^{-3}	0.0269
Max value of A (μm^2)	0.4015	0.4015
Mean P (μm)	1.293	1.616
Sample standard deviation of P (μm)	0.962	0.949
Standard error of estimate for P (μm)	0.0419	0.0487
Total scanned P (μm)	682.87	614.19
Min value of P (μm)	0.096	0.515
Max value of P (μm)	5.791	5.791
Correlation coefficient	0.929	0.869
Estimated fractal dimension D	1.44	1.47
Standard deviation of D	0.02	0.03

range of almost three orders of magnitude in cluster area. The scaling perimeter-area behavior means that there is no characteristic length scale between 0.1 μm and 10 μm in the linear size of the normal phase cluster. Whatever the shape and size of the clusters may be, all points fall closely on the same straight line in logarithmic scale, so that there are no apparent kinks or crossovers on the graph. This enables the fractal dimension D of the cluster perimeter to be estimated from the slope of the regression line of the form of Eq. (7); thus a least-squares treatment of the perimeter-area data for the primary sampling gives an estimate of $D=1.44\pm0.02$ with correlation coefficient 0.929.

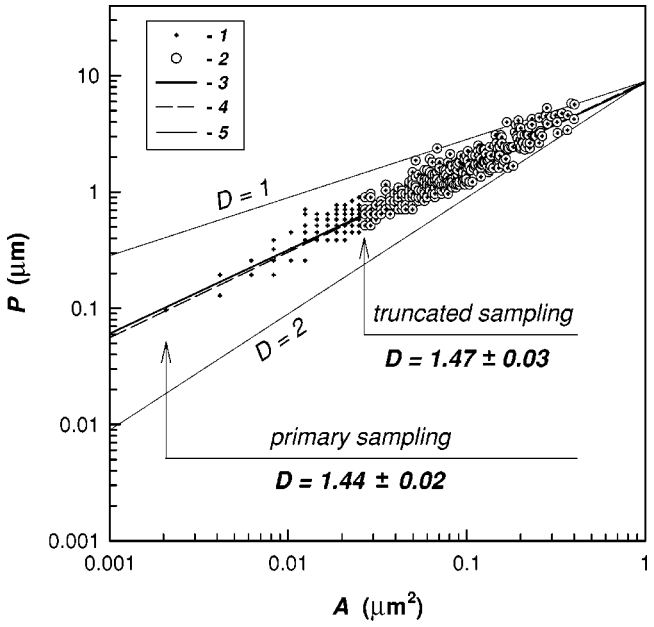

FIG. 2. Perimeter-area relationship for the normal phase clusters with fractal boundary. Plot (1) shows the data of the primary sampling (528 points), plot (2) shows the data of the truncated sampling (380 points), line (3) is the least-squares regression line for the primary sampling, and line (4) is the least-squares regression line for the truncated sampling. Two lines (5) display the range of slope that the perimeter-area curves can have for any possible fractal dimension D ($D=1$ for clusters of Euclidean boundary, $D=2$ for clusters of boundary with the maximum fractality).

This point—that the value found of the coastline fractal dimension differs appreciably from unity—engages great attention. What this means is that the fractal properties of the cluster boundary are of prime importance here. Two straight lines (5) in Fig. 2 bound the range of the slopes that the dependences of the perimeter on the cluster area can have for any arbitrary fractal dimension. The least slope corresponds to Euclidean clusters ($D=1$); the greatest one relates to clusters of the greatest possible coastline dimension, which is equal to the topological dimension of a smooth surface ($D=2$). Such a fractal dimension is inherent, for example, in Peano curves, which fill the whole plane.[11] Whatever the geometric morphological properties of clusters may be, the slope of their perimeter-area graphs will be always bounded by these two limiting lines.

When we deal with the geometric features of the normal phase clusters, we are considering the cross section of the extended columnar defects by the plane carrying a transport current. Therefore, though normal phase clusters are self-affine fractals,[13,14] it is possible to examine their geometric probability properties in the planar section only, where the boundaries of the clusters are statistically self-similar.

Next, using the relation of Eq. (7) between the fractal perimeter and the area of the cluster, as well as the formula of Eq. (6), we get the following expression for the critical current: $I=\alpha A^{-D/2}$, where α is the form factor. In accordance with starting formulas of Eq. (1) and Eq. (2), the exponential distribution of cluster areas of Eq. (3) gives rise to an exponential-hyperbolic distribution of critical currents:

$$F(i)=\exp\left[-\left(\frac{2+D}{2}\right)^{2/D+1} i^{-2/D}\right], \tag{8}$$

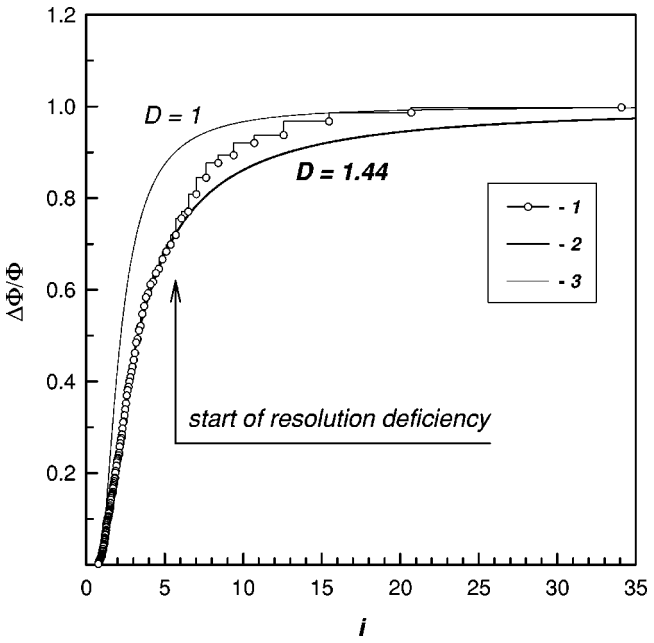

FIG. 3. Effect of a transport current on the magnetic flux trapped in fractal clusters of a normal phase. Step line with open circles (1) is the sample empirical function of the critical current distribution, line (2) shows the decrease in the trapped flux for fractal clusters of coastline dimension $D=1.44$, and line (3) shows the decrease in the trapped flux for Euclidean clusters of coastline dimension $D=1$.

where $i \equiv I/I_c$ is the dimensionless transport current and

$$I_c = \left(\frac{2}{2+D}\right)^{(2+D)/2} \alpha(\overline{A})^{-D/2}$$

is the critical current of the resistive transition.

Thus, the geometric probability properties of the normal phase clusters are responsible for the main features of the critical current statistical distribution. In turn, given the distribution of Eq. (8), the change in the trapped magnetic flux caused by the transport current can be found with the aid of Eq. (1). Two of these graphs are displayed in Fig. 3 both for the fractal clusters of coastline dimension $D=1.44$ found above [curve (2)] and for the Euclidean ones [curve (3)].

In order to get the relationship between the dynamics of the trapped magnetic flux and geometric morphological properties of the superconducting structure, the sample empirical function $F^*=F^*(i)$ of the distribution of the critical currents has been computed. This function gives a statistical estimate of the cumulative probability function $F=F(i)$. First, the empirical distribution function $W^*=W^*(A)$ for the primary sampling of the areas of the normal phase clusters has been found. The value $W^*(A)$ was calculated for each order statistic as the relative number of clusters of area smaller than a given value A. Next, the empirical distribution of the critical currents was computed for the same-order statistics [step line with open circles (1) in Fig. 3] using the following transformations:

$$F^* = 1 - W^*,$$

$$i = \left(\frac{2+D}{2}\right)^{(2+D)/2} \left(\frac{\overline{A}}{A}\right)^{D/2}.$$

Figure 3 shows that in the range of currents $i<6$ the empirical distribution function, which describes the morphological properties of the superconducting structure [plot (1)], coincides ideally with the cumulative probability function [curve (2)] for the coastline fractal dimension of $D=1.44$. Starting with the value of the current $i=6$ the crossover is observed, resulting in the empirical distribution function passing to the dependence for Euclidean clusters ($D=1$). This transition to the Euclidean region is over at large transport currents, when the magnetic flux changes mainly for the breaking of the vortices away from the small clusters (as the smaller clusters have the larger pinning force). The observed crossover has its origin in the finite-resolution capability of measuring the cluster geometric sizes. The distinctive feature of the topologically one-dimensional fractal curve is that its measured length P depends on the measurement accuracy in such a way that $P \propto \delta^{1-D}$, where δ is the yardstick size used to measure this length and $(1-D)$ is the Hausdorff codimension for the Euclidean 1D space.[11] In our case such a fractal curve is represented by the boundary of the normal phase cluster. That is why just the statistical distribution of the cluster areas, rather than their perimeters, is fundamental for finding the critical current distribution of Eq. (8). The topological dimension of the perimeter is equal to unity and does not coincide with its Hausdorff-Besicovitch dimension, which strictly exceeds unity. Therefore the perimeter length of a fractal cluster is not well defined, because its value diverges as the yardstick size is reduced infinitely. On the other hand, the topological dimension of the cluster area is the same as the Hausdorff-Besicovitch one (both are equal to 2). Thus, the area restricted by the fractal curve is a well-defined finite quantity.

Taking into account the effect of the measurement accuracy, the perimeter-area relationship of Eq. (7) can be rewritten as

$$P(\delta) \propto \delta^{1-D} [A(\delta)]^{D/2}, \tag{9}$$

which holds true when the yardstick length δ is small enough to measure accurately all boundaries of the smallest cluster in the sampling. When the resolution is deficient, the Euclidean part of the perimeter length will dominate the fractal one, so there is no way to find the fractal dimension using the scaling relation of Eq. (9). It means that if the length of a fractal curve was measured too roughly with a very large yardstick, its fractal properties could not be detected, and therefore such a geometric object would manifest itself as an Euclidean one. It is just a resolution deficiency of this kind occurs at the crossover point in Fig. 3. Starting with the cluster area less than 0.023 μm^2 (corresponding to the currents of $i>6$) it is impossible to measure all ''skerries'' and ''fjords'' on the cluster coastlines, whereas all the clusters of area less than the size of the measuring cell (3.6×10^{-3} μm^2, which relates to the currents of $i>23$) exhibit themselves as objects of Euclidean boundaries ($D=1$). This resolution deficiency can be also observed in Fig. 2: some crosses at its lower left corner are arranged discretely with spacing equal to the limit of resolution (60 nm), because

some marks for smallest clusters coincide because of the finite resolution of the picture digitization procedure.

The coastline fractal dimension was found above by means of regression analysis of the whole primary sampling, where very small clusters of sizes lying at the breaking point of the resolution limit were also included. Therefore, it is necessary to control how much the estimated value of the fractal dimension could be distorted by the presence of such small clusters in that sampling. For this purpose the truncated sampling has been formed in such a way that only 380 clusters of area greater than 0.0269 μm^2, for which the resolution deficiency has not appeared, have been selected from the primary sampling. The corresponding points are plotted as open circles (2) in Fig. 2, whereas the results of a statistical treatment of this truncated sampling are presented in the third column of Table I. The least-squares estimation of these perimeter-area data gives a value of coastline fractal dimension of $D=1.47\pm0.03$ with correlation coefficient 0.869. The slope of the regression line for the truncated sampling [dotted line (4) in Fig. 2] is slightly steeper than for the primary one [solid line (3)]. It is natural because the presence in the primary sampling of small clusters, which exhibit themselves as Euclidean ones at the given resolution, leads to underrating the magnitude found of the fractal dimension. Nevertheless, the values of fractal dimensions found for both samplings virtually do not differ within the accuracy of the statistical estimation. This is due to the high robustness of the procedure of the fractal dimension estimation on the basis of the scaling relation of Eq. (7): all points both for the primary sampling and for the truncated one fall on the same straight line, without any bends or breaks (see Fig. 2). At the same time, it is necessary to note that the empirical distribution function approach (see Fig. 3) provides the most data-sensitive technique of estimating the resolution capability required to study the fractal properties of clusters.

III. PINNING GAIN FOR THE MAGNETIC FLUX TRAPPED IN FRACTALLY BOUNDED CLUSTERS OF A NORMAL PHASE

The cumulative probability function of Eq. (8) found allows us to fully describe the effect of the transport current on the trapped magnetic flux. Using this function, the probability density $f(i)\equiv dF/di$ for the critical current distribution can be readily derived:

$$f(i)=2/D\left(\frac{2+D}{2}\right)^{2/D+1} i^{-2/D-1} \times\exp\left[-\left(\frac{2+D}{2}\right)^{2/D+1} i^{-2/D}\right]. \tag{10}$$

This function is normalized to unity over all possible positive values of the critical current. The use of the exponential-hyperbolic critical current distribution of Eq. (8) allows us to avoid the inevitable uncertainty caused by truncation of nonphysical negative values of depinning currents, as takes place, for example, in the case of a normal distribution.[51,52]

The exponential-hyperbolic distribution of Eq. (8) has such an important property: the function $F=F(i)$ is extremely "flat" in the vicinity of the coordinate origin. It is easy to show that all its derivatives are equal to zero at the point of $i=0$:

$$\frac{d^k}{di^k}F(0)=0 \quad \text{for any value of} \quad k.$$

Therefore even the Taylor series expansion in the vicinity of the origin converges to zero, instead of the quantity F itself. This mathematical feature has a clear physical meaning: so small a transport current does not affect the trapped magnetic flux because there are no pinning centers of such small critical currents in the overall statistical distribution, so that all the vortices are still too strongly pinned to be broken away. As can be seen from Fig. 3, the change in the magnetic flux becomes appreciable after the transition into a resistive state only (in the transport current range of $i>1$).

The relative change in the trapped flux $\Delta\Phi/\Phi$, which can be calculated from Eq. (8), also defines the density of vortices, n, broken away from the pinning centers by the current i:

$$n(i)=\frac{B}{\Phi_0}\int_0^i f(i')di'=\frac{B}{\Phi_0}\frac{\Delta\Phi}{\Phi}, \tag{11}$$

where B is the magnetic field and $\Phi_0\equiv hc/(2e)$ is the magnetic flux quantum (h is Planck's constant, c is the velocity of light, and e is the electron charge). The graph of the change in the trapped flux as a function of transport current, which is shown in Fig. 3, coincides qualitatively with the curves obtained in experiments on the magnetization of YBCO films subjected to current pulses.[23,24] Figure 3 also displays such a practically important property of superconducting structure containing fractal clusters of a normal phase: the fractality intensifies the magnetic flux trapping, hindering its breaking away from pinning centers, and thereby enhances the critical current which the sample is capable of withstanding, remaining in a superconducting state. Really, the transport current of magnitude $i=2$ causes 43% of the total trapped magnetic flux to break away from the usual Euclidean clusters [curve (3)], whereas this value is equal only to 25% for fractal normal phase clusters of coastline dimension $D=1.44$ [curve (2)]. It is equivalent to a pinning reinforcement of 73% in the latter case. Thus the pinning amplification due to the fractality can be characterized by the pinning gain factor

$$k_D\equiv\frac{\Delta\Phi(D=1)}{\Delta\Phi(\text{current value of } D)},$$

which is equal to the relative decrease in the fraction of magnetic flux broken away from fractal clusters of coastline dimension D compared to the case of Euclidean ones ($D=1$). This quantity can be calculated from the following formula:

$$k_D=\exp\left[\left(\frac{2+D}{2}\right)^{2/D+1} i^{-2/D}-\frac{3.375}{i^2}\right].$$

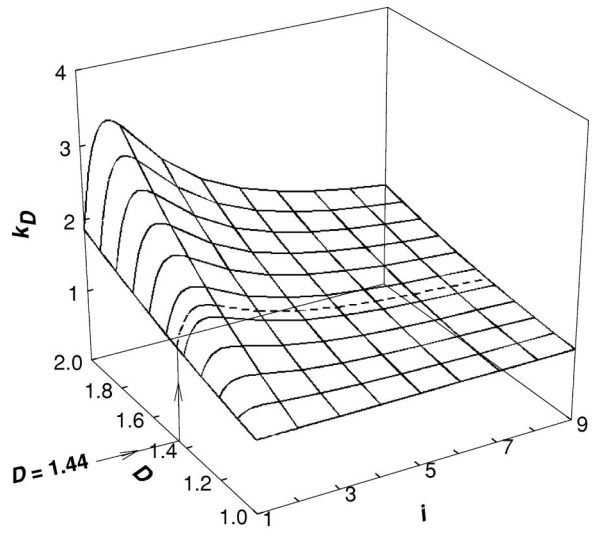

FIG. 4. Pinning gain for an arbitrary coastline fractal dimension of the cluster perimeter.

The characteristic dependences of the pinning gain on the transport current as well as on the fractal dimension are given in Fig. 4. The highest amplification is reached when the cluster boundaries have the greatest possible fractality: $\max_D k_D = k_2 = \exp[(4i-3.375)/i^2]$, with the maximum of k_2 at transport current $i=1.6875$. Let us note that the pinning gain characterizes the properties of a superconductor in the range of the transport currents corresponding to a resistive state ($i>1$). At smaller current the total trapped flux remains unchanged (see Fig. 3) for a lack of pinning centers of such small critical currents, so the breaking away of the vortices has not started yet. When the vortices start to leave the normal phase clusters and move through the weak links, their motion induces an electric field, which, in turn, creates a voltage drop across the sample. Thus, at a transport current greater than the current of the resistive transition some finite resistance appears, so that the passage of electric current is accompanied by energy dissipation. The motion of each depinned vortex causes local heating. As for any hard superconductor (type II, with pinning centers) this dissipation does not mean the destruction of phase coherence yet. Some dissipation always accompanies any motion of a magnetic flux that can happen in a hard superconductor even at low transport current. Therefore the critical current in such materials cannot be specified as the greatest nondissipative current. The superconducting state collapses only when the growth of dissipation becomes avalanche-like as a result of thermomagnetic instability.

The principal reason for pinning enhancement due to the fractality of the normal phase clusters lies in the fundamental properties of the critical current distribution. Figure 5 demonstrates the peculiarities of the fractal probability density specified by Eq. (10). As in Fig. 2, the thin lines show the extreme cases of Euclidean clusters ($D=1$) and clusters of boundaries with maximum fractality ($D=2$). As may be clearly seen from these graphs, the bell-shaped curve of the distribution broadens out, moving towards greater magnitudes of current as the fractal dimension increases. This shift

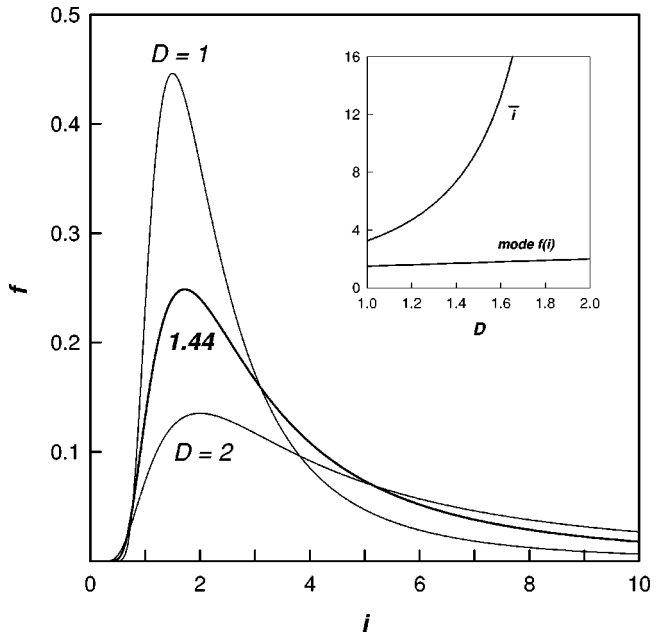

FIG. 5. Influence of the fractal dimension of the perimeter of normal phase clusters on the critical current distribution. The inset shows the dependences of the average critical current $\overline{i}$ and mode *mode* $f(i)$ of this distribution on the coastline fractal dimension.

can be described by the dependences of the average and mode of the critical current distribution on the fractal dimension, as is shown in the inset of Fig. 5. The mode of the distribution, which is equal to the value of the critical current that provides the maximum of the probability density of Eq. (10), depends linearly on the fractal dimension: *mode* $f(i) = (2+D)/2$. The average critical current obeys a much more strong superlinear law specified by Euler gamma function:

$$\overline{i} = \left(\frac{2+D}{2}\right)^{(2+D)/2} \Gamma\left(1-\frac{D}{2}\right).$$

The mean value of the critical current for Euclidean clusters is equal to $\overline{i}(D=1) = (3/2)^{3/2}\sqrt{\pi} = 3.2562$, while for clusters of maximum fractality this value becomes infinite: $\overline{i}(D=2) \to \infty$. Figure 5 clearly demonstrates that increasing the fractal dimension gives a growth of the contribution made by clusters of greater critical current to the overall distribution, resulting just in an enhancement of the magnetic flux trapping.

IV. ELECTRIC FIELD IN THE RESISTIVE STATE

By virtue of the fact that any motion of the magnetic flux causes energy dissipation in superconductors, the question of how such a process could be prevented, or only suppressed, is of prime practical importance. The study of resistive state peculiarities leads to conclusions on the influence of the cluster fractality on the electric field induced by the flux motion. In the resistive state the hard superconductor is adequately specified by its *V-I* characteristic. The critical current distribution of Eq. (10) allows us to find the electric field arising from the magnetic flux motion after the vortices have been

broken away from the pinning centers. Inasmuch as each normal phase cluster contributes to the total critical current distribution, the voltage across a superconductor $V=V(i)$ is the response to the sum of effects made by the contribution from each cluster. Such a response can be expressed as a convolution integral

$$V=R_f\int_0^i (i-i')f(i')di', \tag{12}$$

where R_f is the flux flow resistance. A similar approach is used universally to consider the behavior of clusters of pinned vortex filaments;[53] and to analyze the critical scaling of V-I characteristics of superconductors,[52] that is to say, in all the cases where the distribution of the depinning currents occurs. The present consideration will be primarily concentrated on the consequences of the fractal nature of the normal phase clusters specified by the distribution of Eq. (10), so all the problems related to the possible dependence of the flux flow resistance R_f on the transport current will not be taken up here.

Let us consider the simplest case wherein all of the pinning centers would have an identical critical current i_c, so all the vortices would be broken away simultaneously at $i=i_c$. Then, referring to Eq. (11), their density would have the following form:

$$n=\frac{B}{\Phi_0}\int_0^i \delta(i'-i_c)di'=\frac{B}{\Phi_0}h(i-i_c),$$

where $\delta(i)$ is the Dirac delta function and

$$h(i)\equiv\begin{cases}1 & \text{for } i\geqslant 0,\\ 0 & \text{for } i<0,\end{cases}$$

is the Heaviside step function.

Thus, the trapped flux would change by 100% at once: $\Delta\Phi/\Phi=h(i-i_c)$. Let us note that in this case $i_c=1$ due to the convenient normalization chosen above: $i\equiv I/I_c$.

In the model case of a δ-shaped distribution of the critical currents the voltage across a superconductor in the flux flow regime, according to Eq. (12), would obey the simple linear law $V=R_f(i-i_c)h(i-i_c)$. The corresponding V-I characteristic is shown in Fig. 6 by the dotted line (1).

For the fractal distribution of critical currents the situation is quite different, because the vortices are being broken away now in a wide range of transport currents. After substitution of the function of Eq. (10) into Eq. (12), upon integration by parts, the voltage across a superconductor can be expressed with the cumulative probability function of Eq. (8):

$$V=R_f\int_0^i F(i')di', \tag{13}$$

integration of which gives

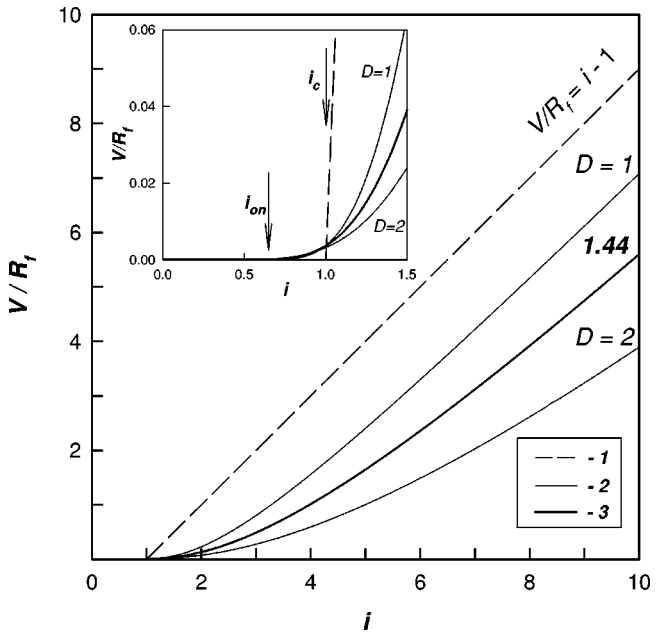

FIG. 6. Voltage-current characteristics of superconductors containing fractal clusters of a normal phase. Dotted line (1) corresponds to the δ-shaped distribution of the critical currents, lines (2) to the extreme dependences of the voltage across a superconductor on the transport current in the case of Euclidean clusters ($D=1$) and clusters of boundaries with maximum fractality ($D=2$), and line (3) to the V-I characteristic of the superconductor containing normal phase clusters of fractal dimension of the perimeter $D=1.44$. The inset shows the region near the resistive transition in an enlarged scale. The initial dissipative range between i_{on} and i_c is clearly seen.

$$V=R_f\exp\left[-\left(\frac{2+D}{2}\right)^{2/D+1} i^{-2/D}\right] \times\left\{i-\left(\frac{2+D}{2}\right)^{(2+D)/2} U\left[\frac{D}{2},\frac{D}{2},\left(\frac{2+D}{2}\right)^{2/D+1} i^{-2/D}\right]\right\}, \tag{14}$$

where $U(a,b,z)$ is Tricomi confluent hypergeometric function.

In extreme cases for $D=1$ and for $D=2$ the expression of Eq. (14) can be simplified (see Appendix B):

(a) Euclidean clusters ($D=1$):

$$V=R_f\left[i\exp\left(-\frac{3.375}{i^2}\right)-\sqrt{3.375\pi}\,\mathrm{erfc}\left(\frac{\sqrt{3.375}}{i}\right)\right], \tag{15}$$

where $\mathrm{erfc}(z)$ is the complementary error function.

(b) Clusters of boundary with the maximum fractality ($D=2$):

$$V=R_f\left[i\exp\left(-\frac{4}{i}\right)+4\mathrm{Ei}\left(-\frac{4}{i}\right)\right], \tag{16}$$

where $\mathrm{Ei}(z)$ is the exponential integral function.

The V-I characteristics of a superconductor containing fractal normal phase clusters are presented in Fig. 6. All the curves virtually start with the transport current value of $i=1$, which agrees with the beginning of the resistive state found above from cumulative probability function of Eq. (8). When the current increases the trapped flux remains unchanged until the vortices start to break away from the pinning centers. As long as the magnetic flux does not move, no electric field is arisen. Two thin lines (2), calculated using the formulas of Eq. (15) and Eq. (16), bound the region the V-I characteristics can fall within for any possible values of fractal dimension. As an example, curve (3) demonstrates the V-I characteristic of a superconductor containing fractal clusters of previously obtained coastline dimension $D=1.44$.

The inset of Fig. 6 shows the region of resistive transition under magnification. As may be seen from this graph, the critical current i_c is preceded by some initial region of the finite voltage drop starting with i_{on}, so the resistive transition of the V-I characteristic is not absolutely abrupt. The magnitude of this onset current i_{on} is determined by the finite resolution along the ordinate axis rather than having some threshold value. The existence of this initial section on the V-I characteristic arises from the tail of the distribution of Eq. (10) in the range of small currents, where the breaking of vortices away from the large clusters occurs. A similar region of initial dissipation has been observed by Prester *et al.*[8,17] in HTS–normal-metal (BPSCCO-Ag) composite tapes.

Figure 6 shows that the fractality reduces appreciably the electric field arising from the magnetic flux motion. This effect is especially strong in the range of the currents $1<i<3$, where the pinning enhancement has a maximum as well (see also Fig. 4). Both these effects have the same nature, inasmuch as their cause consists in the peculiarities of the fractal distribution of critical currents of Eq. (10). As is seen from Fig. 5, an increase of fractality causes a significant broadening of the tail of the distribution $f=f(i)$. It means that more and more small clusters, which can best trap the magnetic flux, are being involved in the process. Hence the density of vortices broken away from pinning centers by the Lorentz force is reducing, so the smaller part of the magnetic flux can flow, creating a smaller electric field. In turn, the smaller the electric field is, the smaller is the energy dissipated when the transport current passes through the sample. Therefore, the decrease in the heat evolution, which could cause a transition of the superconductor into a normal state, means that the current-carrying capability of the superconductor containing such fractal clusters is enhanced.

Thus, Fig. 6, as well as Fig. 4, obviously demonstrates such a practically important result: the fractality of the boundary of the normal phase clusters, which act as pinning centers, prevents the destruction of superconductivity by a transport current and, therefore, causes the critical current to increase.

V. CONCLUSION

Thus, the fractal properties of normal phase clusters have an essential influence on the dynamics of the trapped magnetic flux. The crucial change of the critical current distribution caused by increasing the coastline fractal dimension of the normal phase clusters forms the basis of this effect. The most important result is that the fractality of cluster boundaries strengthens the flux pinning and thereby hinders the destruction of superconductivity by the transport current, resulting in an enhancement of the current-carrying capability of a superconductor. This phenomenon provides possibilities for increasing the critical current value of composite superconductors by optimizing their geometric morphological properties.

APPENDIX A: GEOMETRIC PROBABILITY ANALYSIS OF THE DISTRIBUTION OF ENTRY POINTS INTO WEAK LINKS OVER THE PERIMETER OF A NORMAL PHASE CLUSTER

In the most general way the problem of the entry point into a weak link distribution can be treated in terms of path integrals.[54]

The random distribution of entry points over the perimeter can vary from one cluster to another, so that each normal phase cluster has an entry point distribution function $\psi(l)$ of its own, which belongs to some function class Ω. Here l is the coordinate measured along the cluster perimeter. The probability distribution of functions $\psi(l)$ over all clusters can be characterized by the functional $\Pr\{\psi(l)\}$, which is equal to the probability of finding a given function $\psi(l)$.

The most probable function of the entry point distribution can be expressed by the path integral

$$\Psi(l)\equiv\overline{\psi(l)}=\int_{(\Omega)}\mathcal{D}\psi(l)\,\psi(l)\Pr\{\psi(l)\}, \tag{A1}$$

which gives the mean over all functions of class Ω.

The path integral Fourier transform on the probability functional $\Pr\{\psi(l)\}$ represents the characteristic functional[54]

$$H[k(l)]=\frac{\int_{(\Omega)}\mathcal{D}\psi(l)\exp[i\oint dl k(l)\psi(l)]\Pr\{\psi(l)\}}{\int_{(\Omega)}\mathcal{D}\psi(l)\Pr\{\psi(l)\}}, \tag{A2}$$

where $k(l)$ is the element of the reciprocal function space, and integration in the kernel is carried out over the cluster perimeter: $l\in(0,P)$.

In the simplest case, when all clusters are of an equal entry point distribution, which coincides with the most probable one of Eq. (A1), the probability functional $\Pr\{\psi(l)\}$ is zero for all $\psi(l)$ that differ from $\Psi(l)$, whereas $\Pr\{\Psi(l)\}=1$. As this takes place the characteristic functional of Eq. (A2) becomes

$$H[k(l)]=\exp\left[i\oint dl k(l)\Psi(l)\right]. \tag{A3}$$

If all entry points had fixed coordinates l_j instead of the random ones, their distribution would be $\psi(l)=\beta\Sigma_{j=1}^{N}\delta(l-l_j)$ where N is the number of entry points along the perim-

eter of the cluster involved and $\delta(l)$ is the Dirac delta function. The constant β is being chosen to normalize $\psi(l)$ to unity: $\oint dl\,\psi(l)=1$, so that $\beta N=1$.

Now suppose that all the points of entries into weak links are randomly distributed with uniform probability over the cluster perimeter, so the probability of finding any jth point within some interval dl_j is proportional to its length. In that case the characteristic functional of Eq. (A2) takes the form

$$H[k(l)]=\frac{\oint\ldots\oint\Pi_{j=1}^{N}dl_j\exp[i\beta\Sigma_{j=1}^{N}\oint dlk(l)\,\delta(l-l_j)]}{\oint\ldots\oint\Pi_{j=1}^{N}dl_j}=\frac{1}{P^N}\prod\nolimits_{j=1}^{N}\oint dl_j e^{i\beta k(l_j)}=Q^N, \tag{A4}$$

where

$$Q\equiv\frac{1}{P}\oint dl e^{i\beta k(l)}. \tag{A5}$$

Expanding the function $e^{i\beta k(l)}$ in a power series at $N\gg 1$, and taking into account the condition $\beta N=1$, we may write

$$Q=\exp\left[i\frac{\beta}{P}\oint dlk(l)\right],$$

which, after substitution into Eq. (A4), gives

$$H[k(l)]=\exp\left[i\beta\frac{N}{P}\oint dlk(l)\right]. \tag{A6}$$

The found characteristic functional of Eq. (A6) found has the form of Eq. (A3) with the entry point distribution function

$$\Psi(l)=\frac{1}{P}. \tag{A7}$$

This means that all clusters have the same uniform distribution of the entry points of Eq. (A7), for which the probability of finding a weak link at any point of the perimeter is independent of its position.

The uniform distribution of entry points into weak links can be considered as the realization of a Poisson random process. If the mean number of entry points $\overline{N}$ along the cluster perimeter is large enough ($\overline{N}\gg 1$), then expressions for the characteristic functional of Eq. (A6) as well as for the distribution function of Eq. (A7) remain unchanged.

In the case of a Poisson distribution the entry points are arranged along the perimeter randomly and uniformly with constant concentration $n=\overline{N}/P$ per unit perimeter length. Then, for a preset point located on the perimeter at the coordinate l the probability to find the entry point within the interval $(l,l+\Delta l)$ is equal to $n\Delta l+o(\Delta l)$, where $o(\Delta l)$ is infinitesimal compared with Δl.

The characteristic functional for the Poisson distribution[54] has the form

$$H[k(l)]=\sum_{N}\frac{(Q\overline{N})^N}{N!}e^{-\overline{N}}=e^{\overline{N}(Q-1)},$$

which, after substitution of the expression for Q of Eq. (A5), becomes

$$H[k(l)]=\exp\left[n\oint dl(e^{i\beta k(l)}-1)\right].$$

If we expand $e^{i\beta k(l)}$ in a series anew, for clusters of a large mean number of entry points ($\overline{N}\gg 1$) we get

$$H[k(l)]=\exp\left[i\beta\frac{\overline{N}}{P}\oint dlk(l)\right],$$

which coincides again with the characteristic functional of Eq. (A3) for the entry point distribution function $\Psi(l)=1/P$, which is common to all the clusters.

It is significant that the function of Eq. (A7) gives the isotropic distribution of entry points over the perimeter. This enables the role of fractality of the cluster boundaries to be emphasized, because it is known[4] that anisotropy suppresses the fractal flux penetration in the superconducting area.

APPENDIX B: ELECTRIC VOLTAGE ACROSS A SUPERCONDUCTOR CAUSED BY MAGNETIC FLUX MOTION IN THE EXTREME CASES OF EUCLIDEAN CLUSTERS AND CLUSTERS OF MAXIMUM FRACTALITY

In order to obtain the expressions of Eqs. (14)–(16) for the voltage across a superconductor, it is necessary to integrate the cumulative probability function for the critical current distribution of Eq. (8). The substitution of an exponential-hyperbolic distribution of Eq. (8) in Eq. (13) gives

$$\frac{V}{R_f}=\int_0^i dx\exp(-Cx^{-2/D}),\quad\text{where}\quad C\equiv\left(\frac{2+D}{2}\right)^{2/D+1}. \tag{B1}$$

Using the change of variable of the form $y\equiv Cx^{-2/D}$, we can get the following expression:

$$\frac{V}{R_f}=\frac{D}{2}C^{D/2}\int_{Ci^{-2/D}}^{\infty}dye^{-y}y^{-(2+D)/2},$$

which, upon integration by parts, becomes

$$\frac{V}{R_f}=i\exp(-Ci^{-2/D})-C^{D/2}\Gamma\left(1-\frac{D}{2},Ci^{-2/D}\right), \quad \text{(B2)}$$

where $\Gamma(\nu,z)\equiv\int_z^{\infty}dye^{-y}y^{\nu-1}$ is the incomplete gamma function. This function can be represented as

$$\Gamma(\nu,z)=e^{-z}U(1-\nu,1-\nu,z), \quad \text{(B3)}$$

where $U(a,b,z)\equiv[\Gamma(a)]^{-1}\int_0^{\infty}dye^{-zy}y^{a-1}(1+y)^{b-a-1}$ is the Tricomi confluent hypergeometric function and $\Gamma(a)\equiv\int_0^{\infty}dye^{-y}y^{a-1}$ is the Euler gamma function.

Thus, with the help of Eq. (B3), the expression for the voltage across a superconductor of Eq. (B2) can be written in its final form

$$\frac{V}{R_f}=\exp(-Ci^{-2/D})\left[i-C^{D/2}U\left(\frac{D}{2},\frac{D}{2},Ci^{-2/D}\right)\right]. \quad \text{(B4)}$$

This formula is similar to the expression of Eq. (14). The corresponding V-I characteristic of a superconductor calculated using this expression at $D=1.44$ is shown in Fig. 6 by curve (3).

Equation (B4) can be transformed into a more simple form in two special cases:

(a) For clusters of Euclidean boundary ($D=1$): At $D=1$ the following representation is valid for Tricomi confluent hypergeometric function:

$$U\left(\frac{1}{2},\frac{1}{2},z\right)=\sqrt{\pi}e^{z}\mathrm{erfc}(\sqrt{z}),$$

where $\mathrm{erfc}(z)\equiv(2/\sqrt{\pi})\int_z^{\infty}dye^{-y^2}$ is the complementary error function. The substitution of this representation into Eq. (B4) gives the same expression for the voltage across a superconductor as the formula of Eq. (15):

$$\frac{V}{R_f}=i\exp\left(-\frac{C}{i^2}\right)-\sqrt{\pi C}\,\mathrm{erfc}\left(\frac{\sqrt{C}}{i}\right), \quad \text{(B5)}$$

where, according to Eq. (B1), $C=3.375$.

(b) For clusters of boundaries with maximum fractality ($D=2$): At $D=2$ there is such a representation for the Tricomi confluent hypergeometric function:

$$U(1,1,z)=-e^{z}\mathrm{Ei}(-z),$$

where $\mathrm{Ei}(-z)\equiv\int_{-\infty}^{-z}dy\frac{e^{y}}{y}$, $z>0$, is the exponential integral function. Taking into account this formula, the expression (B4) for the voltage across a superconductor can be rewritten as

$$\frac{V}{R_f}=i\exp\left(-\frac{C}{i}\right)+C\mathrm{Ei}\left(-\frac{C}{i}\right), \quad \text{(B6)}$$

where, according to Eq. (B1), $C=4$. The last formula coincides with the expression of Eq. (16).

The formulas of Eqs. (B5) and (B6) describe the dependences of the voltage across a superconductor in a resistive state on the transport current for extreme values of the coastline fractal dimension. Two corresponding V-I curves are shown in Fig. 6 by thin lines (2). Whatever the geometric morphological properties of the normal phase clusters may be, the V-I characteristics of a superconductor will fall within the region bounded by those two limiting curves, as is shown in Fig. 6 [like curve (3) drawn for $D=1.44$].

*Electronic address: yurk@shuv.ioffe.rssi.ru; iourk@mail.ru FAX: +7 812 2471017.

[1] T. Higuchi, S. I. Yoo, and M. Murakami, Phys. Rev. B **59**, 1514 (1999); Ch. Jooss, R. Warthmann, H. Kronmüller, T. Haage, H.-U. Habermeier, and J. Zegenhagen, Phys. Rev. Lett. **82**, 632 (1999); L. Krusin-Elbaum, G. Blatter, J. R. Thompson, D. K. Petrov, R. Wheeler, J. Ullmann, and C. W. Chu, *ibid.* **81**, 3948 (1998).

[2] S. N. Dorogovtsev and Yu. I. Kuzmin, Phys. Lett. A **170**, 245 (1992).

[3] R. Surdeanu, R. J. Wijngaarden, R. Griessen, C. Rossel, Z. F. Ren, and J. H. Wang, Physica C **282-287**, 2219 (1997).

[4] R. Surdeanu, R. J. Wijngaarden, B. Dam, J. Rector, R. Griessen, C. Rossel, Z. F. Ren, and J. H. Wang, Phys. Rev. B **58**, 12 467 (1998).

[5] M. R. Beasley, in *Percolation, Localization and Superconductivity*, Vol. 109 of *NATO Advanced Study Institute, Series B: Physics*, edited by A. M. Goldman and S. A. Wolf (Plenum Press, New York, 1984), pp. 115–143.

[6] E. Mezzetti, R. Gerbaldo, G. Ghigo, L. Gozzelino, B. Minetti, C. Camerlingo, A. Monaco, G. Cuttone, and A. Rovelli, Phys. Rev. B **60**, 7623 (1999).

[7] C. J. Olson, C. Reichhardt, and F. Nori, Phys. Rev. Lett. **80**, 2197 (1998).

[8] M. Prester, Phys. Rev. B **60**, 3100 (1999).

[9] Yu. I. Kuzmin, Phys. Lett. A **267**, 66 (2000).

[10] B. B. Mandelbrot, Science **155**, 636 (1967).

[11] B. B. Mandelbrot, *Fractals: Form, Chance, and Dimension* (Freeman, San Francisco, 1977).

[12] B. B. Mandelbrot, *The Fractal Geometry of Nature* (Freeman, San Francisco, 1982).

[13] B. B. Mandelbrot, in *Fractals in Physics*, edited by L. Pietronero and E. Tosatti (North-Holland, Amsterdam, 1986), pp. 3–28.

[14] J. Feder, *Fractals* (Plenum Press, New York, 1988).

[15] A. Sidorenko, C. Surgers, T. Trappmann, and H. von Lohneysen, Phys. Rev. B **53**, 11 751 (1996).

[16] R. B. Laibowitz, R. F. Voss, and E. I. Alessandrini, in *Percolation, Localization and Superconductivity* (Ref. 5), pp. 145–160.

[17] M. Prester, P. Kováč, and I. Hušek, Proc. SPIE **3481**, 60 (1998); M. Prester, Supercond. Sci. Technol. **11**, 333 (1998).

[18] S. Alexander, Phys. Rev. B **27**, 1541 (1983); D. C. Hong, H. E. Stanley, A. Coniglio, and A. Bunde, *ibid.* **33**, 4564 (1986); A. S. Skal, Mod. Phys. Lett. B **12**, 727 (1998).

[19] R. Pike and H. E. Stanley, J. Phys. A **14**, L169 (1981); Y. Gefen,

A. Aharony, and S. Alexander, Phys. Rev. Lett. **50**, 77 (1983); R. Rammal and G. Toulouse, J. Phys. (Paris) Lett. **44**, L13 (1983); S. Havlin and D. Ben-Avraham, Adv. Phys. **36**, 695 (1987).

[20] M. Prester, cond-mat/9911458 (unpublished).

[21] M. Baziljevich, A. V. Bobyl, H. Bratsberg, R. Deltour, M. E. Gaevski, Yu. M. Galperin, V. Gasumyants, T. H. Johansen, I. A. Khrebtov, V. N. Leonov, D. V. Shantsev, and R. A. Suris, J. Phys. (Paris) IV **6**, C3-259 (1996).

[22] D. R. Nelson and V. M. Vinokur, Phys. Rev. B **48**, 13 060 (1993); L. Krusin-Elbaum, L. Civale, G. Blatter, A. D. Marwick, F. Holtzberg, and C. Field, Phys. Rev. Lett. **72**, 1914 (1994).

[23] Yu. I. Kuzmin and I. V. Plechakov, Pis'ma Zh. Tekh. Fiz. **25**, 30 (1999) [Tech. Phys. Lett. **25**, 475 (1999)].

[24] Yu. I. Kuzmin, I. V. Pleshakov, and S. V. Razumov, Fiz. Tverd. Tela (St. Petersburg) **41**, 1739 (1999) [Phys. Solid State **41**, 1594 (1999)].

[25] D. Stauffer, Phys. Rep. **54**, 2 (1979).

[26] G. Blatter, M. V. Feigel'man, V. B. Geshkenbein, A. I. Larkin, and V. M. Vinokur, Rev. Mod. Phys. **66**, 1125 (1994); X. Y. Cai, A. Gurevich, I-Fei Tsu, D. L. Kaiser, S. E. Babcock, and D. C. Larbalestier, Phys. Rev. B **57**, 10 951 (1998).

[27] D. J. Scalapino, Phys. Rep. **250**, 329 (1995).

[28] M. J. M. E. de Nivelle, G. J. Gerritsma, and H. Rogalla, Phys. Rev. Lett. **70**, 1525 (1993); H. Pastoriza, S. Candia, and G. Nieva, *ibid.* **83**, 1026 (1999); H. Küpfer, Th. Wolf, A. A. Zhukov, and R. Meier-Hirmer, Phys. Rev. B **60**, 7631 (1999).

[29] H. R. Kerchner, D. P. Norton, A. Goyal, J. D. Budai, D. K. Christen, D. M. Kroegeer, M. Paranthaman, D. F. Lee, F. A. List, R. Feenstra, and E. H. Brandt, Phys. Rev. B **60**, 6878 (1999); R. Haslinger and R. Joynt, *ibid.* **61**, 4206 (2000).

[30] A. I. Rykov, S. Tajima, F. V. Kusmartsev, E. M. Forgan, and Ch. Simon, Phys. Rev. B **60**, 7601 (1999).

[31] I. Maggio-April, C. Renner, A. Erb, E. Walker, and O. Fisher, Nature (London) **390**, 487 (1997).

[32] J. Z. Liu, Y. X. Jia, R. N. Shelton, and M. J. Fluss, Phys. Rev. Lett. **66**, 1354 (1991).

[33] C. A. Duran, P. L. Gammel, R. Wolfe, V. J. Fratello, D. J. Bishop, J. P. Rice, and D. M. Ginsberg, Nature (London) **357**, 474 (1992).

[34] C. A. Duran, P. L. Gammel, D. J. Bishop, J. P. Rice, and D. M. Ginsberg, Phys. Rev. Lett. **74**, 3712 (1995).

[35] R. J. Wijngaarden, R. Griessen, J. Fendrich, and W.-K. Kwok, Phys. Rev. B **55**, 3268 (1997).

[36] W. K. Kwok, U. Welp, G. W. Crabtree, K. G. Vandervoort, R. Hulscher, and J. Z. Liu, Phys. Rev. Lett. **64**, 966 (1990); E. M. Gyorgy, R. B. van Dover, L. F. Schneemeyer, A. E. White, H. M. O'Bryan, R. J. Felder, J. V. Waszczak, and W. W. Rhodes, Appl. Phys. Lett. **56**, 2465 (1990).

[37] M. Oussena, P. A. J. de Groot, S. J. Porter, R. Gagnon, and L. Taillefer, Phys. Rev. B **51**, 1389 (1995); M. Oussena, P. A. J. de Groot, K. Deligiannis, A. V. Volkozub, R. Gagnon, and L. Taillefer, Phys. Rev. Lett. **76**, 2559 (1996).

[38] M. Turchinskaya, D. L. Kaiser, F. W. Gayle, A. J. Shapiro, A. Roytburd, V. Vlasko-Vlasov, A. Polyanskii, and V. Nikitenko, Physica C **216**, 205 (1993); U. Welp, T. Gardiner, D. Gunter, J. Fendrich, G. W. Crabtree, V. K. Vlasko-Vlasov, and V. I. Nikitenko, *ibid.* **235-240**, 241 (1994).

[39] H. Safar, S. Foltyn, H. Kung, M. P. Maley, J. O. Willis, P. Arendt, and X. D. Wu, Appl. Phys. Lett. **68**, 1853 (1996).

[40] U. Welp, T. Gardiner, D. O. Gunter, B. W. Veal, G. W. Crabtree, V. K. Vlasko-Vlasov, and V. I. Nikitenko, Phys. Rev. Lett. **74**, 3713 (1995).

[41] A. Kilic, K. Kilic, and S. Senoussi, J. Appl. Phys. **84**, 3254 (1998); Th. Schuster, H. Kuhn, M. R. Koblischka, H. Theuss, H. Kronmüller, M. Leghissa, M. Kraus, and G. Saemann-Ischenko, Phys. Rev. B **47**, 373 (1993); Th. Schuster, H. Kuhn, E. H. Brandt, M. V. Idenbom, M. R. Koblischka, and M. Konczykowski, *ibid.* **50**, 16 684 (1994).

[42] J. E. Sonier, R. F. Kiefl, J. H. Brewer, D. A. Bonn, S. R. Dunsiger, W. N. Hardy, R. Liang, R. I. Miller, D. R. Noakes, and C. E. Stronach, Phys. Rev. B **59**, R729 (1999).

[43] Yu. I. Kuzmin, Phys. Lett. A **281**, 39 (2001).

[44] Yu. I. Kuzmin, Pis'ma Zh. Tekh. Fiz. **26**, 81 (2000) [Tech. Phys. Lett. **26**, 791 (2000)].

[45] F. Spitzer, *Principles of Random Walk* (Princeton University Press, Princeton, 1964).

[46] C. W. Gardiner, *Handbook of Stochastic Methods* (Springer-Verlag, Berlin, 1983).

[47] V. V. Bryksin, A. V. Goltsev, S. N. Dorogovtsev, Yu. I. Kuzmin, and A. N. Samukhin, J. Phys.: Condens. Matter **4**, 1791 (1992).

[48] H. Fangohr, S. J. Cox, and P. A. J. de Groot, cond-mat/0104455, Phys. Rev. B (to be published).

[49] A. Barone and G. Paternò, *Physics and Applications of the Josephson Effect* (Wiley, New York, 1982).

[50] A. Coniglio and H. E. Stanley, Phys. Rev. Lett. **52**, 1068 (1984).

[51] R. Wördenweber, Phys. Rev. B **46**, 3076 (1992); Yu. I. Kuzmin, A. P. Paugurt, I. V. Pleshakov, and S. V. Rasumov, Supercond. Sci. Technol. **7**, 41 (1994).

[52] B. Brown, Phys. Rev. B **61**, 3267 (2000).

[53] W. H. Warnes and D. C. Larbalestier, Appl. Phys. Lett. **48**, 1403 (1986).

[54] R. P. Feynman and A. R. Hibbs, *Quantum Mechanics and Path Integrals* (McGraw-Hill, New York, 1965).